Dynamic response of graphene to thermal impulse

Jingchao Zhang, Xiaopeng Huang, Yanan Yue, Jianmei Wang, and Xinwei Wang

Phys. Rev. B **84**, 235416 — Published 1 December 2011

DOI: 10.1103/PhysRevB.84.235416

Dynamic response of graphene to thermal impulse

Jingchao Zhang[1], Xiaopeng Huang[1], Yanan Yue[1], Jianmei Wang[2], Xinwei Wang[1,3,*]

[1]2010 Black Engineering Building, Department of Mechanical Engineering,

Iowa State University, Ames, IA 50011, USA

[2]Department of Energy and Power Engineering, Wuhan University, P.R. China

[3]School of Environmental and Municipal Engineering, Qingdao Technological University, P. R. China

A transient molecular dynamics technique is developed to characterize the thermophysical properties of two-dimensional graphene nanoribbons (GNRs). By directly tracking the thermal relaxation history of GNR that is heated by a thermal impulse, we are able to determine its thermal diffusivity fast and accurate. We study the dynamic thermal conductivity of different length GNRs of 1.99 nm width. Quantum correction is applied in all the temperature calculations and is found to have a critical role in thermal transport study for graphene. The calculated specific heat of GNR agrees well with that of graphite at 300.6 and 692.3 K, showing little effect of the unique graphene structure on its ability to store thermal energy. Strong size effect on GNR's thermal conductivity is observed and its theoretical values for infinite length limit are evaluated by data fitting and extrapolation. With infinite length, the 1.99 nm wide GNR has a thermal conductivity of 149 W m^{-1} K^{-1} at 692.3 K, and 317 W m^{-1} K^{-1} at 300.6 K. Our study of the temperature distribution and evolution suggests that diffusive

* Corresponding author. Email: xwang3@iastate.edu. Phone: 515-294-2085. Fax: 515-294-3261.

transport is dominant in the studied GNRs. Non-Fourier heat conduction is observed at the beginning of thermal relaxation procedure. Thermal waves in GNR's in-plane direction are observed only for phonons in the flexural direction (ZA mode). The observed propagation speed (c = 4.6 km s^{-1}) of the thermal wave follows the relation of $c = v_g / \sqrt{2}$ (v_g: ZA phonon group velocity). Our thermal wave study reveals that in graphene the ZA phonons transfer thermal energy much faster than longitudinal (LA) and transverse (TA) modes. Also ZA↔ZA energy transfer is much faster than the ZA↔LA/TA phonon energy transfer.

I. INTRODUCTION

Graphene is a monolayer of graphite arranged in a honeycomb lattice of sp^2 bonded carbon atoms[1] and it has attracted much attention due to its extraordinary electronic and thermal properties[2-5] over the past decade. Graphene nanoribbon (GNR), which is a narrow strip (typically < 20 nm) of graphene, also becomes the subject of significant research because of extraordinary electrical, thermal, and mechanical properties with significant application potential in future nanoelectronic and mechanical devices. The distinguished properties of GNRs have been extensively studied both theoretically and experimentally,[2, 6-9] which indicate that GNRs are a promising material for nanoelectronic applications. Owing to the edge effect and quantum confinement, GNRs are expected to exhibit outstanding thermal properties.[10]

Both experimental and numerical methods have been conducted to study the thermal properties of GNR and ultra-high thermal conductivity has been observed.[11, 12] Recent measurements of the thermal conductivity (k) of a partially suspended graphene sheet revealed a thermal conductivity as high as 5300 W m^{-1} K^{-1} at room temperature (RT).[11] Other experiments[12] suggest graphene has thermal conductivity of 3000–5000 W m^{-1} K^{-1} for a length l of ~10 μm. This high thermal conductivity exceeds that of graphite and is partly attributed to the long phonon mean free path (MFP) in carbon nanostructures. Several research groups[10, 13] using the Brenner potential and non-equilibrium molecular dynamics (NEMD) simulations found much lower values of k in the order of several hundreds of W m^{-1} K^{-1} depending on the width, edge type (armchair or zigzag), and roughness. First principle calculations by Nika *et al*.[14] and Kong *et al*.[15] obtained k values of graphene in the range of 2000–6000 W m^{-1} K^{-1}. In several previous MD simulation investigations, however, the results turned out to be contradictory to that study.

Hu *et al*.[16] calculated the thermal conductivity of GNRs (up to ~4 nm wide and ~10 nm long) around 2000 W m^{-1} K^{-1}. The size of GNRs explored by Hu *et al.* is much smaller than graphene's phonon mean free path (MFP), which is about 775 nm at RT.[12] Therefore the thermal conductivity result in Hu's work is much higher than expected since the value is beyond the upper ballistic bounds.[17] It has been pointed out that quantum ballistic transport could not be fully described by MD simulation and violation of the ballistic upper bounds may be observed when calculating thermal conductance.[18] Although thermal properties of GNR have been studied by various approaches, the length effect has not been investigated yet and the size effect has not been well understood. Moreover, almost all previous numerical methods are based on a steady state temperature gradient to calculate the static thermal conductivity. Dynamic response of graphene to thermal impulses has not been explored in the past.

In this work, MD simulation is performed to study the dynamic response of GNR to thermal impulse based on the second generation of Brenner potential.[19] A transient technique is developed to numerically measure the thermal diffusivity of GNR based on its thermal response. This technique features comparable fast MD simulation implementation and low data uncertainty. To study the size effect on dynamic thermal conductivity of GNR, different lengths (from 14.9 nm to 999.9 nm) GNR structures of 1.99 nm width are used. Quantum correction is applied to both GNR's thermal conductivity (k) and specific heat (c_p) calculation. In Section 2 we first introduce the pulsed laser-assisted thermal relaxation (PLTR) technique, from which our numerical method is derived. Details of this numerical method are then discussed with its application to numerically measure GNR's dynamic thermal conductivity. Section 3 provides MD simulation results and our analysis of size effect on GNR's thermal conductivity. Non-

Fourier heat conduction is analyzed in details and thermal wave propagation in GNR's in-plain direction is studied.

II. PHYSICS OF THE DYNAMIC RESPONSE

In MD simulations to determine the thermal conductivity of materials, non-equilibrium and equilibrium techniques can be applied. Traditional numerical methods like non-equilibrium molecular dynamic (NEMD) simulation employs heat sources and sinks to generate temperature gradient for thermal conductivity calculation. Based on the Fourier's law of heat conduction, the thermal conductivity can be calculated from the temperature gradient and heat flux. An alternative approach to determine the thermal conductivity is equilibrium molecular dynamic (EMD) simulation based on the Green-Kubo expression that relates k to the integral over time t of the heat flux autocorrelation function by

$$\lambda = \frac{1}{3Vk_B T^2}\int_0^\infty \langle J(t)\cdot J(0)\rangle dt\,, \tag{1}$$

where k_B is the Boltzmann constant, V the volume, T temperature of the sample, and the angular brackets denote an ensemble average. The thermal conductivity can be calculated using Eq. (1) once the heat flux vector $J(t)$ is known. A detailed comparison of the MD techniques for computing thermal conductivity was conducted by Schelling *et al*.[20] Generally speaking, the NEMD approach requires large temperature gradients which takes relatively long simulation time and has significant boundary condition issues at interfaces. Results calculated by using the EMD method depend sensitively on the initial conditions of each simulation, thus necessitating a large ensemble of simulations. The slow convergence of the autocorrelation function further increases the computational demand, requiring long integration time periods.[21] Therefore in present study, a transient cooling method is developed to evaluate the dynamic thermal

conductivity of GNR with much less computational time requirement while bears higher accuracy.[22]

A. Dynamic method and mathematical model

The numerical method used in our MD simulation process is derived from the pulsed laser-assisted thermal relaxation (PLTR) technique, which is developed by our group to measure the thermal diffusivity of one-dimensional micro/nanoscale structures in experiment.[22, 23] In the PLTR technique, the to-be-measured sample is suspended over two copper electrodes. When running the experiment, a nanosecond laser pulse is used to irradiate the sample wire uniformly to induce a temperature increase (ΔT). Configuration of this experiment is shown in Fig. 1(a). Right after the pulsed laser heating, temperature of the sample will gradually go down. Temperature evolution of the sample is shown in Fig. 1(b). Such temperature relaxation is strongly determined by the samples' thermal diffusivity and length. From this temperature relaxation history, the thermal diffusivity of the wire can be determined with sound accuracy. In experiment, the length of the wire is significantly greater than its diameter, which will simplify the physical model to one-dimensional. The thermal conductivity is determined via 1D heat transfer equation

$$\frac{\partial \rho c_p T}{\partial t} = k \frac{\partial^2 T}{\partial x^2} + \dot{q}\,, \tag{2}$$

with homogeneous boundary conditions and initial conditions, $T(x = 0, t) = T(x = L, t) = 0$ and $T(x, t = 0) = 0$. Here T only represents the temperature variation induced by the thermal impulse and $\dot{q}$ the rate of thermal energy generation induced by the laser pulse (pulse width: Δt) heating. The solution to the partial differential equation described by Eq. (2) can be obtained from the integral of the Green's function,

$$G_{X11}(x,t|x',\tau)=\frac{2}{L}\sum_{m=1}^{\infty}\exp[-m^2\pi^2\alpha(t-\tau)/L^2]\times\sin(m\pi\frac{x}{L})\sin(m\pi\frac{x'}{L}). \quad (3)$$

The average temperature of the wire $T(t)$ for $0 < t \le \Delta t$ is expressed as

$$T(t)=\frac{1}{L}\int_{x=0}^{L}T(x,t)dx=\frac{8\dot{q}L^2}{k\pi^4}\sum_{m=1}^{\infty}\frac{1-\exp[-(2m-1)^2\pi^2\alpha t/L^2]}{(2m-1)^4}. \quad (4)$$

For time t larger than Δt, we have,

$$T(t)=\frac{8\dot{q}L^2}{k\pi^4}\sum_{m=1}^{\infty}\frac{\exp[-(2m-1)^2\pi^2\alpha t/L^2]\{\exp[(2m-1)^2\pi^2\alpha\Delta t/L^2]-1\}}{(2m-1)^4}. \quad (5)$$

After normalizing as $T^*=[T(t)-T_{\min}]/(T_{\max}-T_{\min})$ (T_{min} is 0 and T_{max} is the maximum temperature increase of the sample calculated as $\dot{q}\Delta t/\rho c_p$), and using the relation $k = \rho c_p \alpha$, where ρ is mass density, c_p specific heat and α thermal diffusivity, the normalized temperature relaxation simplified using Taylor expansions can be written as

$$T^*=\frac{8}{\pi^2}\sum_{m=1}^{\infty}\frac{\exp[-(2m-1)^2\pi^2\alpha t/L^2]}{(2m-1)^2}. \quad (6)$$

Equation (6) shows that for any kind of material of arbitrary length, the normalized temperature relaxation follows the same shape with respect to the Fourier number F_o (= $\alpha t/L^2$).[22, 23] Further convergence study shows that to make the summation in Eq. (6) converge, the value of the term related to m should be less than 10^{-3} of the summation from terms 1 to m-1. When m=15, the summation in Eq. (6) will converge to a stable value with negligible error. The thermal diffusivity of the sample is determined by global data fitting of the temperature relaxation curve. In this method, the normalized temperature decrease is calculated using Eq. (6) by using different trial values of thermal diffusivity. The trial value giving the best fit (least squares) of the experimental data is taken as the sample's thermal diffusivity.

B. Atomic potential and MD domain construction

In our MD simulation, the second generation Brenner potential[19] (REBO) based on the Tersoff potential[24, 25] with interactions between C-C bonds is used. The time step is 0.5 fs for all calculations. To avoid any stretching or compressing stress on the GNR structure, free boundary conditions are applied to the *y* and *z* directions. The simulation domain is bounded with two Lennard-Jones (LJ) walls in the *x* direction that enclose all the atoms. By applying LJ walls to the system, the GNR structure could be fully relaxed during the thermal equilibrium calculation and will not have folding effect. The energy *E* of wall-particle interactions is given by the 9-3 LJ potential

$$E = \varepsilon[\frac{2}{15}(\frac{\sigma}{r})^9 - (\frac{\sigma}{r})^3] \qquad r < r_c \quad , \tag{7}$$

where *r* is the distance from particle to the wall, and ε and σ are the usual LJ parameters, which are set to be 0.00284 eV and 3.4 Å respectively. r_c represents the cutoff distance specified in simulation. The distance from each LJ wall to the GNR plane is set to be 0.335 nm, which is the distance between two neighboring carbon layers in graphite structure. Configuration of the LJ walls is shown in Fig. 2.

Based on the PLTR technique, a numerical method is constructed to investigate the dynamic response of GNR and its thermophysical properties. In MD simulation, a two-dimensional GNR with free boundary conditions is initially created. The GNR used in MD simulation is of half-length compared to that used in PLTR experiment, since MD simulation only applies the transient cooling process to one end of the GNR, while in experiment, both ends of the sample is maintained at RT. In numerical method [Fig. 1(c)], the cooling area of GNR stands for one of the sample-base contact point in the PLTR experiment and the rest part

represents half length of the sample which has been irradiated by a pulsed laser. For example, if the sample used in the PLTR experiment has a length of L, then only a $L/2$ GNR structure needs to be built in the simulation, which significantly reduces the computational time. The system is first heated to a higher temperature (325 K in our work) and reaches thermal equilibrium state before a cold impulse is added to one end of the GNR. The cooling area [shown in Fig. 1(c)] will maintain at a lower temperature (275 K) so the system will have thermal relaxation and reach thermal equilibrium again. To reach a steady state at 325 K before cooling relaxation starts, a NVT condition is applied to the system for 500 ps. In the following 100 ps, a NVE calculation is performed to assure the system's stability. After thermal equilibrium calculation, four layers of carbon atoms at one end of GNR structure are chosen to form a "cooling group", whose temperature is "rescaled" to a value of 275 K and remains at this value through the relaxation process. The cooling procedure is accomplished by a velocity rescaling approach. The "rescaling" process is only applied to the translational degrees of freedom for all atoms. This is an important consideration since extended spherical or aspherical particles which have rotational degrees of freedom may also reach equilibrium state with this method. To assure total momentum of the system is conserved during this rescaling process, a net velocity from the cooling group atoms is removed from the translational degrees of freedom before thermal rescaling takes place. The relaxation time used to reach a uniform temperature for the system is dependent on the length of GNR and its thermal diffusivity. The data analysis method used in the PLTR technique could also be applied to this numerical approach. From the temperature relaxation history, the thermal diffusivity of GNR can be calculated by global data fitting. .

Compared with the NEMD and EMD approaches, this dynamic method takes much less

time to measure the thermal diffusivity and has significantly reduced data uncertainty since more data points are used in calculation (the average temperature of the whole system is used).

C. **Quantum correction**

In MD simulations, the temperature can be easily calculated from the time average kinetic energy of atoms in the sample section within the simulation time using the energy equipartition theorem:

$$\langle E \rangle = \sum_{1}^{N} \frac{1}{2} m v_i^2 = \frac{3}{2} N k_B T_{MD} , \tag{8}$$

where $\langle E \rangle$ is the mean kinetic energy, v_i the velocity of atoms, m the atomic mass, N the number of atoms in the system and k_B the Boltzmann constant.[26, 27] However, it is worth pointing out that this method is valid only at high temperatures ($T \gg T_D$, T_D is the Debye temperature). When the system temperature is lower than the Debye temperature, it is necessary to apply quantum correction to both the MD temperature and thermal conductivity calculation. In present work, we derived the quantum correction equation for two-dimensional GNR model as

$$T_{MD} = \frac{2}{3} T_{LA} x_{LA}^{-3} \int_0^{x_{LA}} \frac{x^2}{e^x - 1} dx + \frac{2}{3} T_{TA} x_{TA}^{-3} \int_0^{x_{TA}} \frac{x^2}{e^x - 1} dx + \frac{1}{3} T_{ZA} x_{ZA}^{-2} \int_0^{x_{ZA}} \frac{x}{e^x - 1} dx , \tag{9}$$

where T_{MD} is the temperature in MD simulation, T_{LA}, T_{TA}, T_{ZA} are the Debye temperatures of three different acoustic modes in GNR, which are 2840 K, 1775 K, and 1120 K respectively, x_{LA}, x_{TA}, x_{ZA} are the ratios of corrected temperatures (temperatures after quantum correction, denoted as T) and Debye temperatures. Given the values of T_{MD}, which are generated in the MD simulation process, x_{LA}, x_{TA} and x_{ZA} values can be determined by the inverse form of Eq. (9). In our work, first of all, a wide range of T values are substituted into Eq. (9) to get x_{LA}, x_{TA}, x_{ZA}, and calculate the corresponding T_{MD}. After we obtain the relations (a curve) between T_{MD} and T, the

corrected temperatures can be calculated by interpolation based on a specified T_{MD}. Corresponding temperatures are then used to calculate GNR's thermal conductivity and specific heat. Large differences between T_{MD} and T are observed in our work. For example, when T_{MD} decreases from 325 K to 275K in MD simulation, corrected temperatures range from 725.8 K to 658.8 K. It concludes that quantum correction is of great importance in GNR's thermal property calculation.

III. RESULTS AND DISCUSSION

To calculate GNR's thermal diffusivity, initial and final temperatures of the system need to be provided. Therefore, NVE conditions are applied to the system both before and after cooling relaxation. The average temperature values in two NVE calculations are then used as the upper and lower limits in global data fitting. During cooling relaxation, the temperature of GNR's cooling area is kept at 275 K constantly, and temperatures of the rest part are recorded for each time step. Several millions of data sets will be recorded before the system reaches thermal equilibrium. The huge amount of temperature results not only makes it difficult for data analysis, but also induces significant noises to the results. To reduce the impact of this problem, the recorded temperature data are averaged each 100 time steps before global fitting, and so as in the thermal diffusivity and specific heat calculations.

A. Fitting results of GNR and specific heat

In this work, GNRs of different lengths 14.9, 29.6, 59.4, 124.6, 249.6, 499.6, and 999.9 nm are calculated for their thermal diffusivity. The thermal conductivities of all GNRs are calculated with the same MD parameters except the cooling relaxation time. Take 124.6 nm long

GNR as an example, after the system reaches thermal equilibrium at temperature 325 K, a cold impulse is applied and it takes 650 ps for the cooling relaxation process to finish. The quantum-corrected temperature results are then used in global data fitting to determine its thermal diffusivity, which is 2.9×10^{-5} m^2 s^{-1}. After obtaining the thermal diffusivity, the thermal conductivity can be calculated by $k = \rho c_p \alpha$. The thermal conductivity is 95.8 W m^{-1} K^{-1} for 124.6 nm long GNR. Figure 3 shows global fitting curves for GNRs of different lengths As we can see from Fig. 3, with the length of GNR increasing, the MD simulation results will be more identical to theoretical results since more carbon atoms are used in the temperature calculation. Take a closer look at the fitting results in Fig. 3, it is found that the diffusive heat transfer model has a lower temperature than the MD data at the beginning. Then as time goes on, the agreement between them becomes better. Such early stage large difference could be induced by the non-Fourier effect heat conduction and the ballistic effect of phonon thermal transport, which will be discussed later in this paper.

To obtain the dynamic thermal conductivity of GNR, graphene's specific heat needs to be calculated first. Since c_p values are the same for GNR structures around T_{MD} = 300 K, we choose the 59.4 nm GNR model for our study. After 500 ps NVT and 50 ps NVE calculation, the system reaches steady state at 295.5 K. Then a heat flux of 3.3×10^7 W m^{-2} is added to the system continuously for 500 ps. After the heating process, the system reaches steady state at 305.5 K. The temperature rise by this heating is 13.2 K after quantum correction. The specific heat is calculated by $Q = c_p m \Delta T$, where Q is the total energy added to the system, m the total mass of atoms and ΔT the temperature difference with quantum correction. Q is expressed as $Q = q'' A t$, where A stands for the heating area and t the heating time. The specific heat is calculated at 1.528

$\times 10^3$ J kg^{-1} K^{-1} (at 692.3 K after quantum correction), which is nearly the same as graphite's specific heat of 1.519×10^3 J kg^{-1} K^{-1} (at 700 K).[28]

B. Thermal transport in GNRs

Ballistic transport has been observed when the phonon mean free path (MFP) is much larger than the size of GNR that contains the medium through which the phonon travels, such that the phonon alters its motion only by hitting against the walls. Recent experiments suggest that thermal transport at the nanoscale is dominated by a ballistic rather than a diffusive mechanism.[12] The power law relationship also implies that graphene conducts heat mainly through ballistic transport mode in a low temperature region.[29]

In this work, however, by comparing the spatial temperature distribution of GNR in MD simulation with the theoretical results calculated from solving diffusive heat conduction equation, we could not see strong ballistic thermal transport in GNR's in-plane direction. It is probably due to the statistical oscillation of the temperature that overshadows the ballistic thermal transport. Based on the diffusive mechanism along the in-plane direction of graphene, the transient heat conduction equation $\partial T/\partial t = \alpha \cdot \partial^2 T/\partial x^2$ (α is thermal diffusivity) is solved by using the explicit method. Since the cooling relaxation curve is dependent on GNR's length and thermal diffusivity, to keep the consistency, initial and boundary conditions used in this calculation are identical with those in the MD simulations, including the α values. A short time step (Δt = 10 fs) and high spatial resolution (Δx = 1 nm) are employed in three different cases (14.9 nm, 59.4 nm and 499.6 nm). The MD simulation results agree well with the theoretical curves derived from diffusive heat conduction equation. It suggests that the thermal transport mechanism in GNR's in-plane

direction is quite close to diffusive situation. The temperature evolutions of GNRs are shown in Fig. 4. Among the three GNR structures, the case for 14.9 nm requires the shortest time to reach the steady state, while the agreement is not as good as the other two due to the lack of sufficient temperature data points in space. GNRs of 59.4 nm and 499.6 nm lengths show a sound agreement between the MD simulation results and theoretical curves. This confirms the point that longer sample length could give more accurate evaluation of the thermal conductivity. Meanwhile, high accuracy for the values of thermal diffusivity derived from the PLTR physical model in MD simulation is assured. Given the fact that the thermal transport inside GNR could mainly be diffusive, Eq. (6), which is used for global fitting of thermal diffusivity, is still within the diffusive limit. However, ballistic effect is still important when GNR length is small. From Fig. 3, it is shown that for short GNR structures, the beginning part of MD simulation results and fitting curves do not match as well as the longer ones, which are mainly induced by ballistic effect (discussed in section 3.4).

C. Size effect on thermal conductivity

To better compare our MD simulation results with previous experimental and numerical data, we also calculated GNRs' dynamic thermal conductivity and specific heat at 300.6 K (after quantum correction). During the cooling relaxation process, the MD temperature decreases from 70 K to 50 K, corresponding 324.8 K to 276.6 K after quantum correction. Take the 124.6 nm GNR as an example, its thermal diffusivity and thermal conductivity values are 4.1×10^{-5} m^2 s^{-1} and 72.6 W m^{-1} K^{-1} respectively. The specific heat of the GNR at 300.6 K is calculated at 827 J kg^{-1} K^{-1}, which is close to graphite's value of 709 J kg^{-1} K^{-1} at the same temperature.[28] Although the thermal diffusivity of GNR is higher at 300.6 K than that at 692.3 K (2.9×10^{-5} m^2 s^{-1}), its

thermal conductivity decreases due to a smaller specific heat. The calculated high values of the thermal conductivity suggest that the MFP in GNR is long even at RT. The latter may result in strong dependence of the thermal conductivity on the length l of the GNR and roughness of its edges since the phonon boundary scattering starts to play a prominent role when l is comparable to MFP. Therefore, the traditional defined thermal conductivity is no longer an intrinsic property of materials. Instead, it changes with the length of materials. There are substantial experimental observations showing the thermal conductivity of thin films is significantly lower than that of bulk materials.[30-32] Figure 5 depicts GNR's thermal diffusivity and conductivity at different length. It can be concluded that dynamic thermal conductivity of GNR increases with its length significantly.

For bulk materials, the kinetic theory gives the relationship between the macroscopic thermal conductivity and microscopic motions[33, 34] as

$$k = \frac{1}{3}\rho c_p v l , \tag{10}$$

where k is the thermal conductivity, ρ the mass density, c_p the specific heat, v the average phonon velocity and l the phonon mean free path, representing the average distance a phonon travels between successive collisions. In this sense, k is the one used in Fourier's law of heat conduction

$$q'' = -k \cdot \nabla T , \tag{11}$$

where q'' is heat flux and T is temperature. Equation (10) is derived with the assumption that the space of particle motion is unbounded and is valid only if phonons can travel very long distance before they hit boundary. Equation (11) is simply a derivative of the more fundamental rule, the Boltzmann Transport Equation, under steady state and quasi-equilibrium conditions.

Given the calculated thermal conductivity results for different GNRs at 692.3 K and 300.6 K, we could derive k values for infinite length GNRs using data fitting. Although it is no longer meaningful to refer to thermal conductivity as a basic physical concept at micro/nanoscales, its effective value is still of great importance from the engineering perspective and is expressed for a film structure as $k_{eff} = q''L / \Delta T$, where q'' is heat flux at steady state in the length direction, L the film length and ΔT the temperature difference across the film. A material-independent relation is proposed as $k_{eff} / k = (1 + P \cdot l / L)^{-1}$, where k is the theoretical thermal conductivity of infinite length GNR, l the average phonon MFP, L the length of GNR sample, P the correlation related to boundary conditions and GNR shape. This equation is a universal relationship applicable in both ballistic and diffusive regimes of heat conduction. Since l is only related to internal scattering, its value for bulk materials can still be used and is calculated using the kinetic theory described by Eq. (10). It is worth noting that Eq. (10) is for three-dimensional and must be adapted as $k = \rho c_p v l / 2$ for two-dimensional situations for GNR, in which the movement and scattering of phonons are confined in a plane. From the above equation, we can get the relationship between l and k for two-dimensional systems as $l = 2k / (\rho c_p v)$. Thus k_{eff} could be expressed as

$$k_{eff} = \frac{k}{1 + 2P \cdot k / (\rho c_p v L)} . \tag{12}$$

To carry out this calculation, only phonon velocity v needs to be specified. According to Holland[35], the following formula is a good approximation of the average phonon velocity within a wide temperature range

$$\frac{1}{v} = \frac{1}{3}\left(\frac{1}{v_L} + \frac{2}{v_T}\right), \tag{13}$$

where v_L and v_T are the longitudinal and transverse sound speeds. Recent research by Nika *et al.*[14] indicates that the measured longitudinal and transverse velocities in graphene are v_L = 21.3 km s^{-1} and v_T = 13.6 km s^{-1} respectively. Using Eq. (13), the calculated average phonon velocity for GNR is 15.5 km s^{-1}. Fitting the calculated thermal conductivity values by using Eq. (12), P and k values are 14 and 149 W m^{-1} K^{-1} respectively at 692.3 K while at 300.6 K, P and k are 20 and 317 W m^{-1} K^{-1} respectively. The fitting results are shown in Fig. 5, and sound agreement is obtained the fitting results and MD data. Majumdar *et al*.[36] derived the relationship between k_{eff}/k and L/l as $k_{eff}/k = \left(1+4l/3L\right)^{-1}$ for 2-dimensional heat conduction situation. This equation is also based on the Boltzmann Transport theory and indicated that P equals 4/3 for diffusive scattering boundary. Our calculated P values of 20 and 14 exceed the upper bound of diffusive scattering. Therefore, the thermal conductivity of GNR has been greatly reduced from the theoretical values and the reduction is not only attributed to boundary scattering, but also other changes induced by phonon frequency, phonon wave length, group velocity of phonons and interactions among phonon branches.

As mentioned above, quantum correction is of great significance in the calculation of GNR's thermal conductivity. Evans *et al.*[37] applied the EMD method to calculate the thermal conductivity of graphene ribbons with dimensions of 2 × 10 nm^2 at around 2000 W m^{-1} K^{-1}. The temperature they used is 300 K, which corresponds to 692.3 K after quantum correction. From Eq. (1) we see that their calculated thermal conductivity would be more than 5 times smaller than their current results if quantum correction is applied. The non-Fourier effect is also observed at

the beginning part of GNR's thermal relaxation process, which reduces GNR's thermal conductivity to some extent. From the above discussion, we can conclude that our calculated thermal conductivity of GNR is within acceptable range compared with previous studies.

D. Ballistic and non-Fourier effect in dynamic response

Most heat conduction problems are described and analyzed using Fourier's law of heat conduction. However, it is well known that for transient problems in an extremely short period of time and very high heat flux, this classical diffusion theory may break down. The dynamic temperature responses under ultra-high speed heating have shown some behavior which could not be predicted by the thermal diffusion theory and many models have been developed to interpret these experiments.[38, 39] Cattaneo and Vernotte formulated a well-known macroscopic description of thermal wave propagation,[40, 41] which is a conventional hyperbolic energy equation expressed as

$$\tau \frac{\partial^2 T}{\partial t^2} + \frac{\partial T}{\partial t} = \alpha \nabla^2 T , \tag{14}$$

where τ is the relaxation time of thermal wave, T and α the temperature and thermal diffusivity. Joseph and Preziosi[38] described the microstructural effects by a relaxation function and decompose it into two relaxation times, which lead to a description of a transient heat conduction equation in the following generalized form,

$$\frac{1}{\alpha}\frac{\partial T}{\partial t} + \frac{\tau_q}{\alpha}\frac{\partial^2 T}{\partial t^2} = \nabla^2 T + \tau_\theta \frac{\partial}{\partial t}(\nabla^2 T) . \tag{15}$$

For dielectric crystals, τ_q and τ_θ represent the relaxation times for momentum-nonconserving and momentum-conserving processes in the phonon system. Comparing Eq. (15) with microscopic models suggest that if τ_q and τ_θ are formulated properly by some microscopic quantities, this

macroscopic model could fully describe the same heat conduction equation as those in microscopic models. Cattaneo-Vernotte's thermal wave law and Fourier's thermal diffusion law are two special cases of this generalized model for $\tau_\theta = 0$ and $\tau_\theta = \tau_q = 0$.

In this work, four layers of carbon atoms at one end of GNR are cooled to a low temperature in several time steps by a velocity rescaling method. The use of this rapid cooling technique leads to an extremely high heat flux adjacent to cooling area and non-Fourier effects have been found to exist at the beginning part of thermal relaxation period (Fig. 3). To explore this non-Fourier mechanism, numerical simulation based on the implicit finite-difference method is employed to study the temperature evolution of GNR and make comparison with the MD result. One-dimensional discretization along the in-plane direction of GNR with spacing $\Delta x = 1\times10^{-2}$ nm is conducted and a small time step with $\Delta t = 5\times10^{-2}$ ps is used. By fitting the MD results of 14.9 nm GNR using Eq. (15), we give the values of τ_q and τ_θ as 1.85 and 1.01 ps respectively. The large value of τ_θ indicates that diffusive heat transfer is significant in GNR's thermal conductivity. The fitting curves are shown in Fig. 6. The thermal diffusivity of 14.9 nm GNR given by this fitting is 1.44×10^{-5} m^2 s^{-1}, which is larger than the value of 9.55×10^{-6} m^2 s^{-1} calculated by the previous pure diffusion model. Tang *et al.*[42] proved that a larger τ_θ will produce a higher rate thermal diffusion effect and results in rapid temperature response in early time. Since our calculated values of τ_q and τ_θ are in the same order, we could conclude that both diffusion conduction and thermal wave conduction are affecting GNR's thermal conductivity strongly at the beginning part. In Fig. 6, it could be seen that the MD temperatures decrease much slower than the diffusive fitting curve at the beginning, which could be explained by the thermal wave effects in non-Fourier thermal conduction.

To better understand the effects induced by the ballistic thermal transport and non-Fourier heat conduction, we plot out the spatiotemporal isothermals of 14.9 nm GNR for both the MD results and numerical results that are calculated from Fourier's diffusive heat equation. The results are shown in Fig. 7. As mentioned above, the GNR system has a cooling impulse of 275 K imposed on a 325 K thermal equilibrium system to calculate the GNR's thermal diffusivity. However, the temperature difference (50 K) is very small compared with the data noise, which makes it difficult to justify the temperature change in isotherms. Therefore, we initially set the GNR system at 700 K to reach thermal equilibrium, and then a cooling impulse of 200 K is added to the cooling area. For the full diffusion calculation, we use the thermal diffusivity at 300 K. The temperature of the cooling area, which is kept at 200 K, is not included in the contours. Figure 7(a) depicts the temperature evolution of MD results from 700 K to 200 K within the first 10 ps. Comparing the low temperature areas (violet and blue regions) in Figs. 7(a) and (b), we notice that at the beginning of the heat conduction, the MD temperature diffuses slower than the numerical results, whereas after around 6 ps, the MD temperature diffuses faster than the numerical results. The temperature differences between the MD and numerical results can be explained by the non-Fourier effect. Figure 6 shows that the diffusive fitting curve decreases faster than the MD data at the beginning, and become flattened after around 6 ps. This is in sound agreement with the results shown in Fig. 7.

To take a further look at GNR's thermal wave propagations, a thermal impulse is imposed upon one end of 14.9 nm GNR. The system is initially kept at 50 K to reach thermal equilibrium. Then four layers of carbon atoms at one end are connected to a Nose-Hoover

thermostat kept at 1000 K for 0.4 ps. The rest part of GNR is divided into 64 unit cells along the length direction, each containing about 20 atoms. The average energy of each unit cell is then used to calculate its temperature. The isotherm contours are shown in Fig. 8. The pictures depict how heat diffuses from the origin through the entire field. In the GNR system, heat is mainly transported by acoustic phonons, while the contribution from high-lying optic branches is small and negligible. Figure 8(b), (c) and (d) show the transverse, longitudinal and flexural component of GNR's thermal waves respectively. Balandin *et al.*[43] calculated lattice thermal conductivity of GNR and conclude that flexural acoustic phonons (ZA) do not make substantial contributions to heat conduction due to their low group velocity. However, recent experiments and theoretical analysis have proved that ZA phonons provide the dominant contribution to GNR's thermal conduction.[44-46] Seol *et al*.[47] carried out full quantum mechanical calculations of the three-phonon scattering processes to obtain the phonon relaxation time for each phonon mode. They calculated the substrate-phonon scattering rate for LA, TA and ZA phonon modes and found that due to the large specific heat value of the ZA mode and large mean phonon scattering time, the ZA mode contribute as high as 77% and 86% at 300 K and 100 K respectively for suspended GNR's thermal conductivity. By formulating the ballistic thermal conductance of phonons in a two-dimensional system and using phonon's dispersion relation, Nakamura *et al*.[48] calculated the contributions of the LA, TA and ZA phonons to graphene's thermal conductance. They conclude that the ballistic phonon conductance is determined by the ZA phonon modes below about 20 K and contributions of the TA and LA phonon modes cannot be neglected above 20 K while the ZA phonon modes are still in dominant. Although much work has been done to analyze ZA mode's effect on GNR's thermal conductivity, however, to our best knowledge, there are no MD simulations have been done to prove this valuable theorem. In present work, we can clearly see

in Fig. 8(d) that a strong thermal wave propagates through the spatiotemporal isotherms (ZA mode), while in Figs. 8(b) and (c) no evident thermal waves are observed. When the thermal relaxation time of phonons is large, the thermal wave effect will be more prominent. Therefore, we conclude that the ZA mode is more significant than LA and TA modes in respect for GNR's thermal conductivity. Also we can conclude that during thermal transport by the ZA phonons, the energy transfer among ZA phonons is much faster than that between ZA and LA/TA phonons. This is because if the ZA↔LA/TA phonon energy exchange is comparable to ZA↔ZA energy exchange, thermal wave could also be observed in the LA and TA temperature evolution. However, no thermal wave is observed in the spatiotemporal isotherms of LA and TA phonon temperatures.

In these spatiotemporal isotherms, group velocities for TA, LA and ZA mode are identified. When the 1000 K thermal impulse is imposed on one end of GNR, a local stress will be generated and will propagate in the in-plane directions. The local temperatures of GNR will remain unchanged until this stress wave arrives and its propagation speed could be measured in Fig. 8. Stress wave fronts are denoted by solid lines in Fig. 8. Since these velocities represent the energy transmission speed in GNR, they are also known as group velocities (v_g). From Fig. 8, the group velocities of TA, LA and ZA modes are calculated at 9.8 km s^{-1}, 9.8 km s^{-1} and 7.0 km s^{-1} respectively. Group velocities could be calculated from GNR's dispersion relation by the expression $v_g = d\omega / dk$, where ω is the angular frequency and k the wave number. Wirtz *et al*.[49] compared GNR's phonon dispersion relations calculated by Dubay *et al*.[50] and Maultzsch *et al*.[51] The result is shown in Fig. 9. From the TA, LA and ZA dispersion relation curves in Fig. 9, different group velocities for each phonon branch can be calculated. On the TA curve from

GNR's dispersion relation, the average group velocities calculated in AB and DF regions are 9.7 km s^{-1} and 9.8 km s^{-1} respectively. For LA mode, EF region contributes to group velocity measured in Fig. 8(c) and the average group velocity in this region is 9.7 km s^{-1}. For the ZA mode, regions AC and FG have average group velocities at 6.8 km s^{-1} and 7.0 km s^{-1} and contribute to the group velocity in Fig. 8(d). Theoretical study of the second sound wave under linear approximation for three-dimensional materials shows that thermal wave propagation velocity is $c = v_g / \sqrt{3}$,[52] where v_g is the group velocity. For two-dimensional GNR, this relation should be modified as $c = v_g / \sqrt{2}$.[53] In Fig. 8(d), the thermal wave propagation velocity is calculated at 4.6 km s^{-1} for the ZA mode, as denoted by the dashed line in Fig. 8(d). Based on the group velocity in Fig. 8(d), the thermal wave speed is predicted at $c = v_g / \sqrt{2} = 7.0 / \sqrt{2} = 4.9$ km s^{-1}. This value agrees well with the thermal wave speed 4.6 km s^{-1} observed in Fig. 8(d).

IV. CONCLUSION

A fast transient technique was developed to characterize the thermophysical properties of GNRs using MD simulation. A Debye model for two-dimensional GNR was derived for temperature's quantum correction. The specific heat of GNRs was calculated by MD simulation and the results are 1528 J kg^{-1} K^{-1} and 827 J kg^{-1} K^{-1} at 692.3 K and 300.6 K. These values are very close to those of graphite, and suggest that the unique 2D structure of graphene has little effect on its ability to store thermal energy. Based on obtained thermal conductivity data at different lengths, the thermal conductivity for infinite length GNRs were calculated at 149 W m^{-1} K^{-1} (692.3 K) and 317 W m^{-1} K^{-1} (300.6 K). These values are much smaller than some data reported in literatures for GNRs of similar width. It reflects the fact that the quantum correction of temperature is critical for thermal transport study of graphene. The calculated thermal

conductivity is reduced by boundary scattering and other property changes due to the restriction of small width (1.99 nm). Non-Fourier heat conduction was observed to be significant in 14.9 nm long GNR and wavelike heat flux is observed in transient heating of GNR system. A thermal wave was only observed for the ZA phonon, suggesting that thermal transport by ZA phonons is faster than that by the TA and LA modes. It is conclusive that the ZA mode is dominant for GNR's thermal conduction. Also the energy transfer among ZA phonons is much faster than that between ZA and LA/TA phonons. The observed propagation speed (c = 4.6 km s^{-1}) of the thermal wave follows the relation of $c = v_g / \sqrt{2}$ where v_g is the ZA phonon group velocity (7.0 km s^{-1} from our calculation).

ACKNOWLEDGEMENTS

This work was partially supported by the U.S. Army Research Office under agreement #W911NF1010381. Also partial support of this work from the National Science Foundation (CBET-0931290, CMMI-1029072, CBET-0932573, and CMMI-0926704) is gratefully acknowledged.

References

[1] A. K. Geim and K. S. Novoselov, Nat Mater **6**, 183 (2007).

[2] Y. W. Son, M. L. Cohen, and S. G. Louie, Nature **444**, 347 (2006).

[3] K. S. Novoselov, A. K. Geim, S. V. Morozov, D. Jiang, Y. Zhang, S. V. Dubonos, I. V. Grigorieva, and A. A. Firsov, Science **306**, 666 (2004).

[4] J. S. Bunch, A. M. van der Zande, S. S. Verbridge, I. W. Frank, D. M. Tanenbaum, J. M. Parpia, H. G. Craighead, and P. L. McEuen, Science **315**, 490 (2007).

[5] Y. Yue, J. Zhang, and X. Wang, Small (2011). doi: 10.1002/smll.201101598

[6] T. Kawai, M. Hino, T. Ebisawa, S. Tasaki, D. Yamazaki, Y. Otake, G. Shirouzu, and N. Achiwa, Physica B **276**, 977 (2000).

[7] A. Rycerz, J. Tworzydlo, and C. W. J. Beenakker, Nat Phys **3**, 172 (2007).

[8] K. Wakabayashi, Y. Takane, and M. Sigrist, Phys Rev Lett **99**, 10 (2007).

[9] T. Yamamoto, S. Watanabe, and K. Watanabe, Phys Rev Lett **92** 075502 (2004).

[10] Z. X. Guo, D. Zhang, and X. G. Gong, Appl Phys Lett **95** 163103 (2009).

[11] A. A. Balandin, S. Ghosh, W. Z. Bao, I. Calizo, D. Teweldebrhan, F. Miao, and C. N. Lau, Nano Lett **8**, 902 (2008).

[12] S. Ghosh, I. Calizo, D. Teweldebrhan, E. P. Pokatilov, D. L. Nika, A. A. Balandin, W. Bao, F. Miao, and C. N. Lau, Appl Phys Lett **92** 151911 (2008).

[13] T. Ouyang, Y. P. Chen, K. K. Yang, and J. X. Zhong, Epl-Europhys Lett **88** 28002 (2009).

[14] D. L. Nika, E. P. Pokatilov, A. S. Askerov, and A. A. Balandin, Phys Rev B **79** 155413 (2009).

[15] B. D. Kong, S. Paul, M. B. Nardelli, and K. W. Kim, Phys Rev B **80** 033406 (2009).

[16] J. N. Hu, X. L. Ruan, and Y. P. Chen, Nano Lett **9**, 2730 (2009).

[17] N. Mingo and D. A. Broido, Phys Rev Lett **95**, 096105 (2005).

[18] Y. Xu, X. B. Chen, B. L. Gu, and W. H. Duan, Appl Phys Lett **95** 233116 (2009).

[19] D. W. Brenner, O. A. Shenderova, J. A. Harrison, S. J. Stuart, B. Ni, and S. B. Sinnott, J Phys-Condens Mat **14**, 783 (2002).

[20] P. K. Schelling, S. R. Phillpot, and P. Keblinski, Phys Rev B **65** 144306 (2002).

[21] S. Berber, Y. K. Kwon, and D. Tomanek, Phys Rev Lett **84**, 4613 (2000).

[22] J. Q. Guo, X. W. Wang, D. B. Geohegan, and G. Eres, Funct Mater Lett **1**, 71 (2008).

[23] J. Q. Guo, X. W. Wang, D. B. Geohegan, G. Eres, and C. Vincent, J Appl Phys **103** 113505 (2008).

[24] B. W. Dodson, Phys Rev B **35**, 2795 (1987).

[25] J. Tersoff, Phys Rev Lett **61**, 2879 (1988).

[26] N. Yang, G. Zhang, and B. W. Li, Nano Lett **8**, 276 (2008).

[27] X. P. Huang, X. L. Huai, S. Q. Liang, and X. W. Wang, J Phys D Appl Phys **42** 095416 (2009).

[28] John Wiley, *Fundamentals of heat and mass transfer* (Hoboken, NJ, 2007).

[29] E. Munoz, J. X. Lu, and B. I. Yakobson, Nano Lett **10**, 1652 (2010).

[30] J. C. Lambropoulos, M. R. Jolly, C. A. Amsden, S. E. Gilman, M. J. Sinicropi, D. Diakomihalis, and S. D. Jacobs, J Appl Phys **66**, 4230 (1989).

[31] S. R. Mirmira and L. S. Fletcher, J Thermophys Heat Tr **12**, 121 (1998).

[32] D. G. Cahill, Microscale Therm Eng **1**, 85 (1997).

[33] J. M. Ziman, Philos Mag **5**, 757 (1960).

[34] S. Volz, J. B. Saulnier, M. Lallemand, B. Perrin, P. Depondt, and M. Mareschal, Phys Rev B **54**, 340 (1996).

[35] M. G. Holland, Phys Rev **132**, 2461 (1963).

[36] A. Majumdar, J Heat Trans-T Asme **115**, 7 (1993).

[37] W. Evans, Appl Phys Lett **96**, 203112 (2010).

[38] D. D. Joseph and L. Preziosi, Rev Mod Phys **61**, 41 (1989).

[39] M. N. Ozisik and D. Y. Tzou, J Heat Trans-T Asme **116**, 526 (1994).

[40] P. Vernotte, Cr Hebd Acad Sci **246**, 3154 (1958).

[41] C. Cattaneo, Cr Hebd Acad Sci **247**, 431 (1958).

[42] D. W. Tang and N. Araki, Mat Sci Eng a-Struct **292**, 173 (2000).

[43] A. A. Balandin, D. L. Nika, S. Ghosh, and E. P. Pokatilov, Appl Phys Lett **94** 203103 (2009).

[44] L. Lindsay, D. A. Broido, and N. Mingo, Phys Rev B **83** 235428 (2011).

[45] L. Lindsay, D. A. Broido, and N. Mingo, Phys Rev B **82** 115427 (2010).

[46] B. W. Li, Z. Q. Wang, R. G. Xie, C. T. Bui, D. Liu, X. X. Ni, and J. T. L. Thong, Nano Lett **11**, 113 (2011).

[47] L. Shi, et al., Science **328**, 213 (2010).

[48] K. Saito, J. Nakamura, and A. Natori, Phys Rev B **76** 115409 (2007).

[49] L. Wirtz and A. Rubio, Solid State Commun **131**, 141 (2004).

[50] O. Dubay and G. Kresse, Phys Rev B **67**, 035401 (2003).

[51] J. Maultzsch, S. Reich, C. Thomsen, H. Requardt, and P. Ordejon, Phys Rev Lett **92** 075501 (2004).

[52] M. Chester, Phys Rev **131**, 2013 (1963).

[53] X. Xu and X. Wang, Appl Phys a-Mater **73**, 107 (2001).

List of Figures

Figure 7 Spatiotemporal isotherms of 14.9 nm GNR with a cooling area located at the lower boundary. (a) MD results, (b) numerical results calculated from Fourier diffusive heat conduction equation. The initial system temperatures for both cases are 700 K, and then a cooling impulse of 200 K is added below the origin area.

Figure 8 Spatiotemporal isotherms of 14.9 nm GNR with a thermal impulse imposed at the lower boundary for 0.4 ps: (a) overall temperature, (b) temperature of transverse phonons, (c) temperature of longitudinal phonons, (d) temperature of flexural phonons. Solid lines represent thermal wave front.

Figure 9 Phonon dispersion relations of graphene based on ab initio calculation.[49] The three phonon dispersion branches, which originate from the Γ point of the first Brillouin zone, correspond to acoustic modes and the rest three branches are for optical modes. The regions that correspond to different group velocities in Fig. 8 are denoted by dashed lines. (with permission from Elsevier for use in this paper)

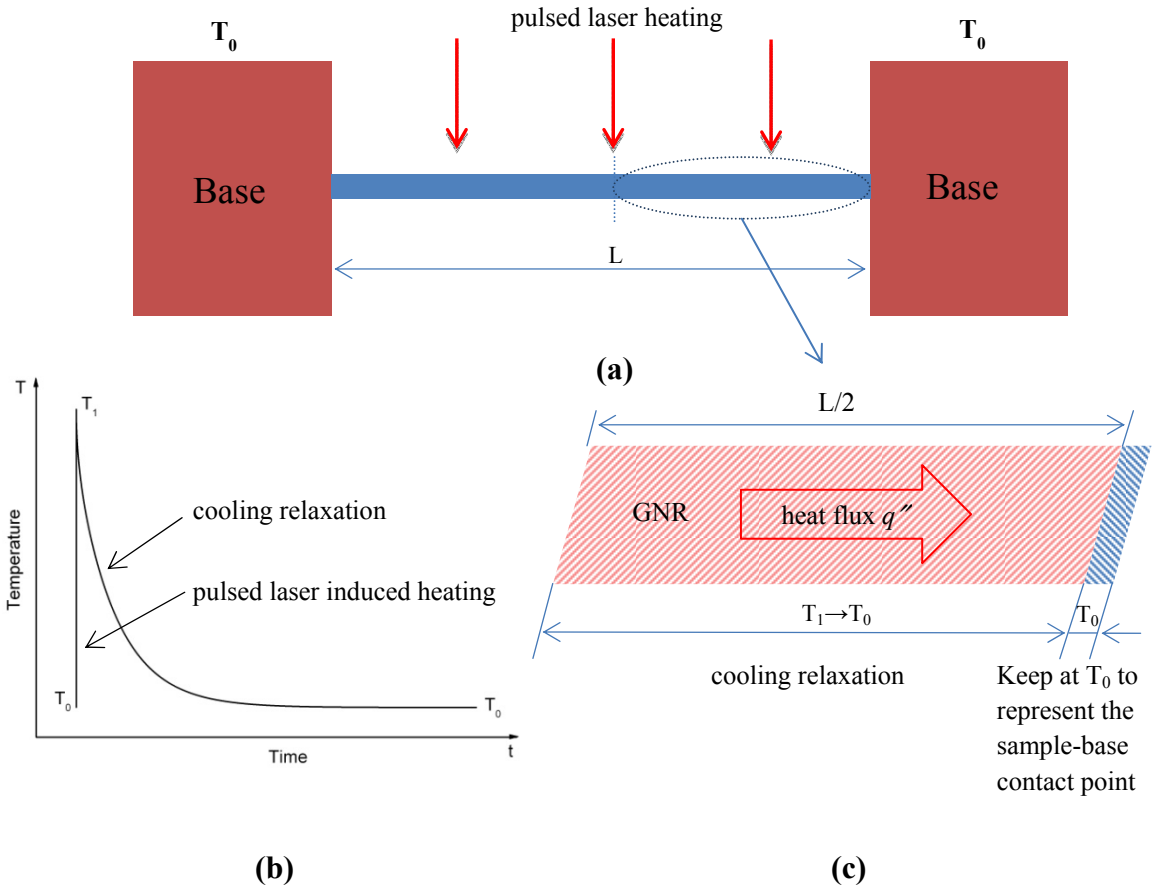

Fig. 1. Schematic of experiment and MD simulation methods for PLTR. (a) A sample is suspended over two electrodes in experiment. The temperature of the two bases is kept at T_0 (RT). (b) Changes of sample temperature after pulsed laser heating. The sample temperature is T_0 at initial state, and then rises to T_1 quickly because of the induced heating by laser pulse. Cooling relaxation continues until sample's temperature reaches T_0 again. (c) Numerical principles derived from the PLTR technique. Temperature of the system is set at T_1 initially. Then one end of the GNR is kept at a low temperature (T_0) to represent the sample base contact point.

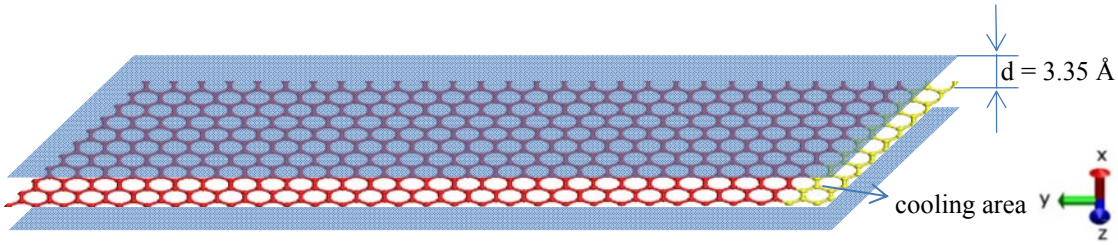

Fig. 2. Structure of LJ walls in the *x* direction. The GNR is placed in the middle of upper and lower LJ walls. The distance between the wall and GNR plane is 3.35 Å.

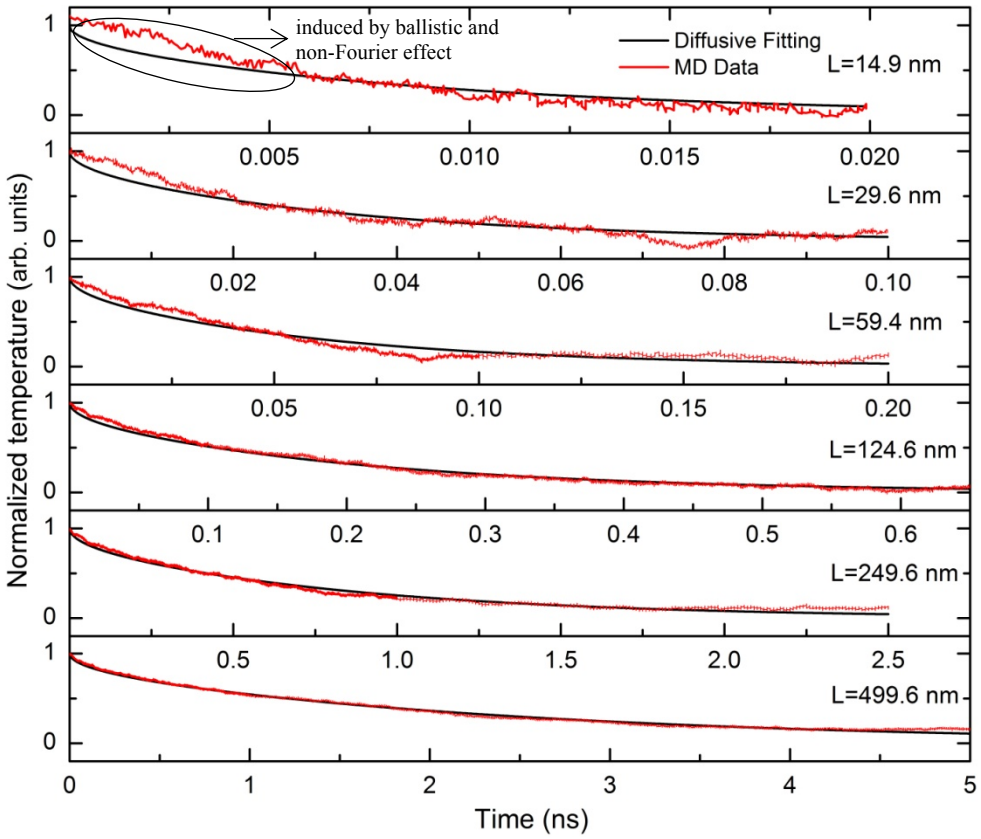

Fig. 3. Global fitting results of different lengths GNRs at 692.3 K. The lengths of GNRs from top to bottom are 14.9 nm, 29.6 nm, 59.4 nm, 124.6 nm, 249.6 nm, and 499.6 nm.

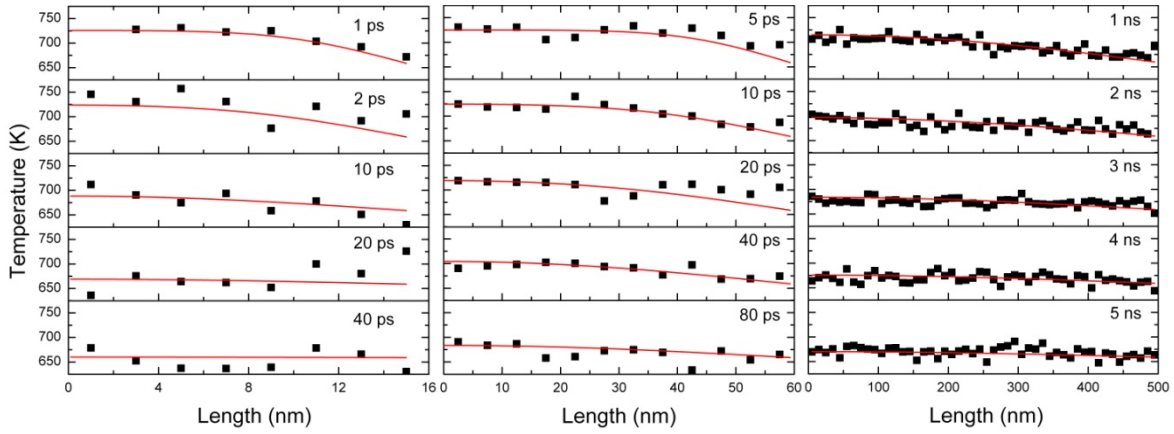

(a) (b) (c)

Fig. 4. Spatial temperature evolution in GNRs at different times. The solid squares stand for MD simulation results and the curves represent theoretical results derived from diffusive heat conduction equation. The GNR length is 14.9 nm, 59.4 nm, and 499.6 nm for figures (a), (b), and (c), respectively.

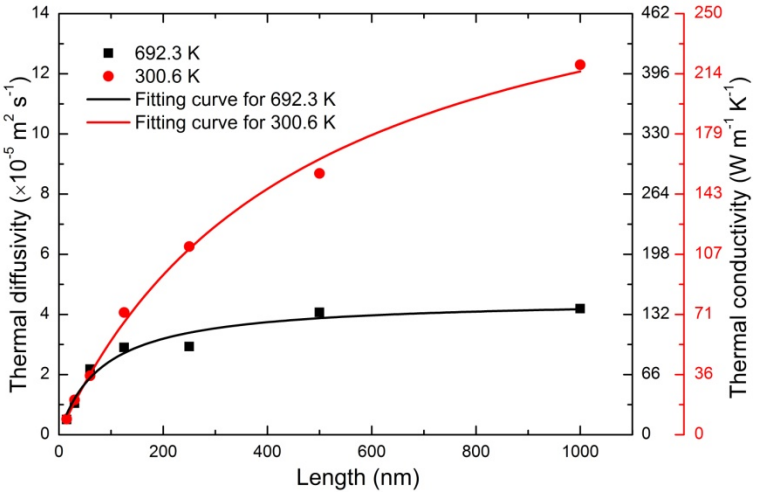

Fig. 5. Thermal diffusivity (α) and thermal conductivity (k) variation against the GNR length.

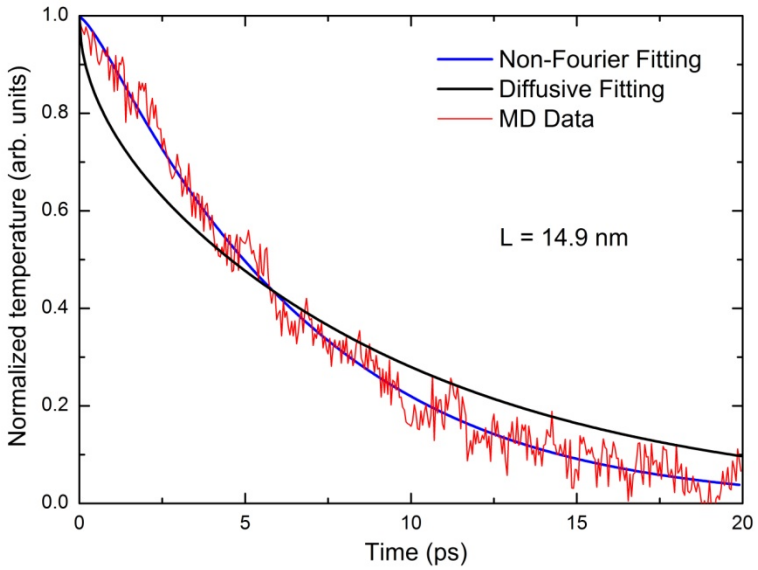

Fig. 6. Comparison of non-Fourier fitting and diffusive fitting to MD data. MD results are above diffusive fitting curve in the first 6 ps due to a decreased effective thermal conductivity induced by the non-Fourier effect. The non-Fourier fitting curve matches MD results soundly by using two relaxation times τ_q and τ_θ.

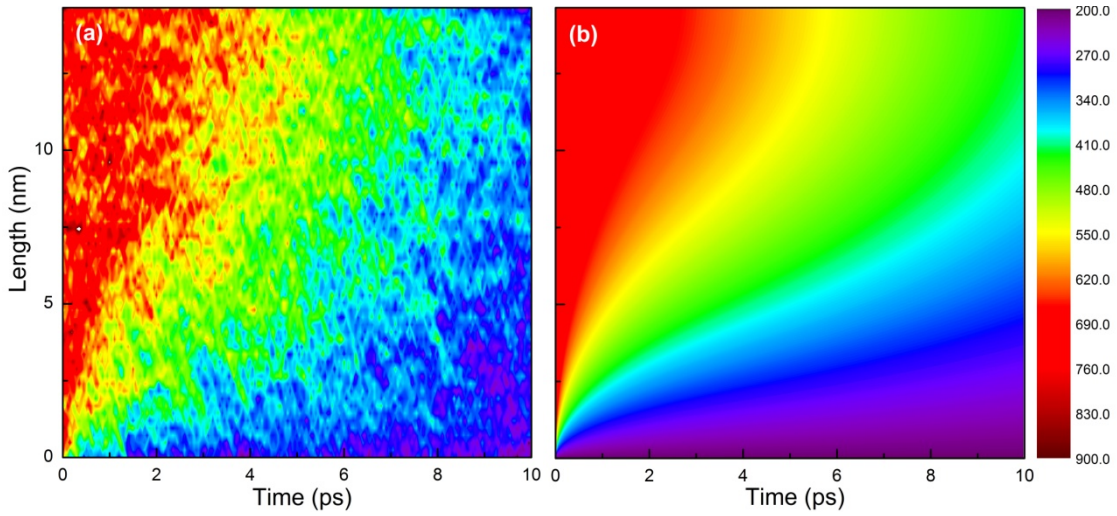

Fig. 7. Spatiotemporal isotherms of 14.9 nm GNR with a cooling area located at the lower boundary. (a) MD results, (b) numerical results calculated from Fourier diffusive heat conduction equation. The initial system temperatures for both cases are 700 K, and then a cooling impulse of 200 K is added below the origin area.

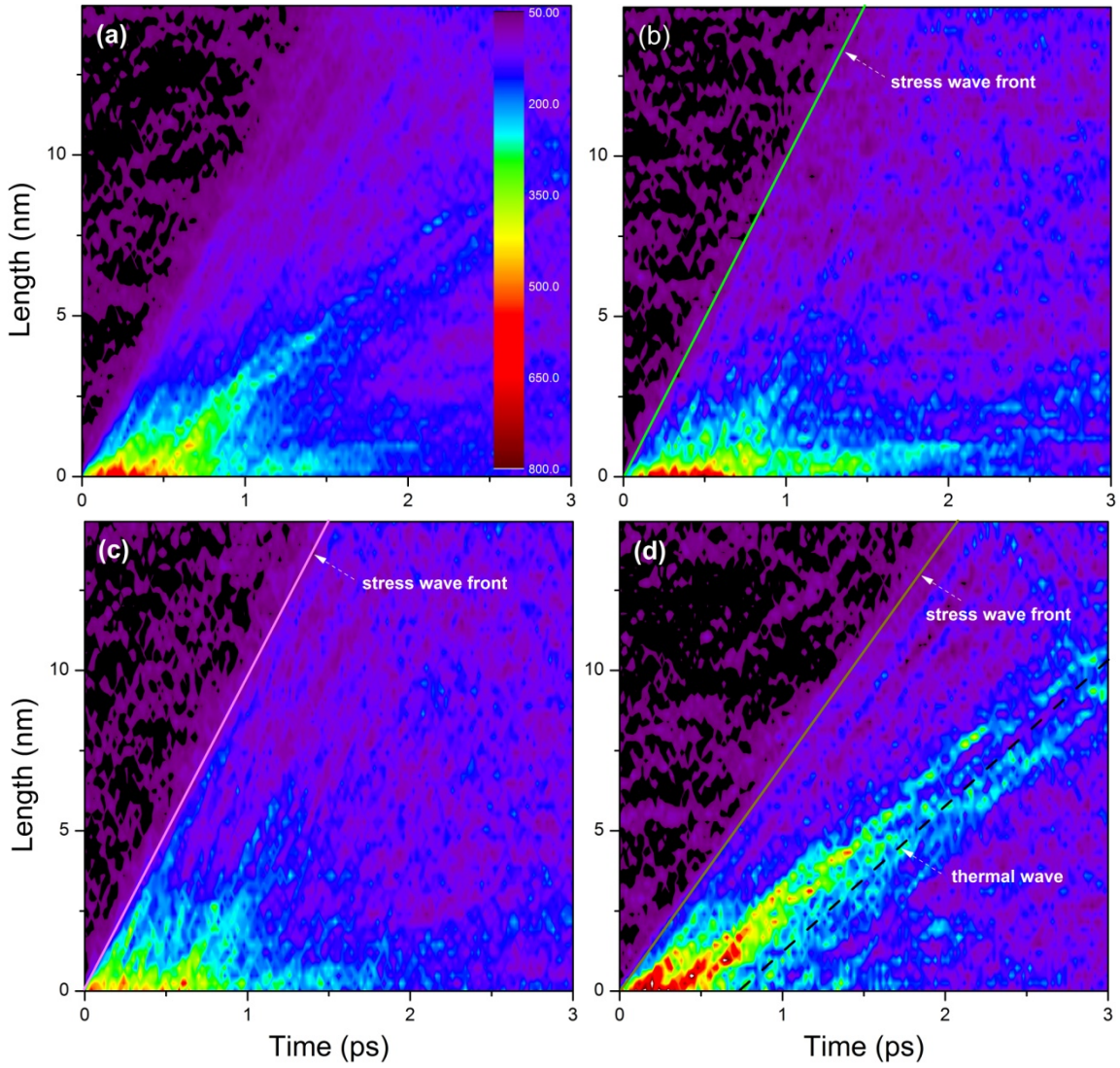

Fig. 8. Spatiotemporal isotherms of 14.9 nm GNR with a thermal impulse imposed at the lower boundary for 0.4 ps: (a) overall temperature, (b) temperature of transverse phonons, (c) temperature of longitudinal phonons, (d) temperature of flexural phonons. Solid lines represent thermal wave front.

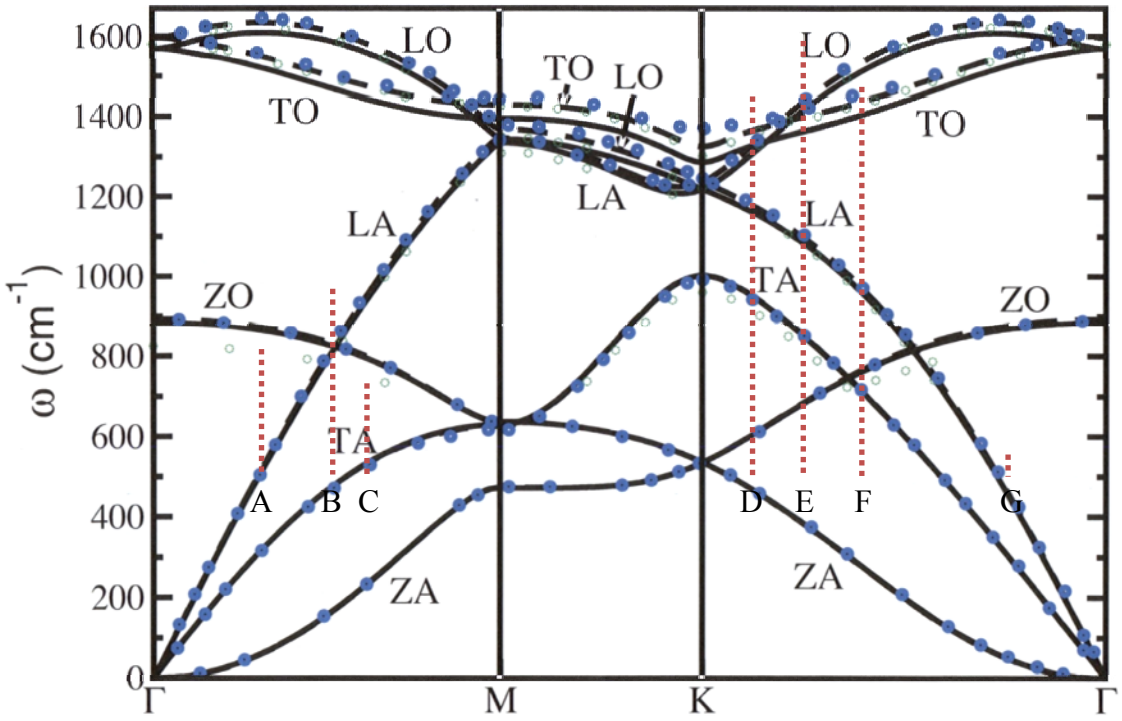

Fig. 9. Phonon dispersion relations of graphene based on ab initio calculation.[49] The three phonon dispersion branches, which originate from the Γ point of the first Brillouin zone, correspond to acoustic modes and the rest three branches are for optical modes. The regions that correspond to different group velocities in Fig. 8 are denoted by dashed lines. (with permission from Elsevier for use in this paper)